Geochimica et Cosmochimica Acta 435 (2026) 57–66

Contents lists available at ScienceDirect

Geochimica et Cosmochimica Acta

journal homepage: www.elsevier.com/locate/gca

N and O isotope fractionation reveals distinct pathways of dissimilatory nitrite reduction to ammonium

Guojun Chen [a,1], Qinqin Hao [a,b,1], Yan Ru [a,c], Andreas Kappler [d,e,f], Raymond Jianxiong Zeng [c], Xiaomin Li [g], Zebin Hong [a], Fanghua Liu [a], Fujun Yue [h], Shiwen Hu [a], Tongxu Liu [a,*]

[a] National-Regional Joint Engineering Research Center for Soil Pollution Control and Remediation in South China, Guangdong Key Laboratory of Integrated Agro-environmental Pollution Control and Management, Institute of Eco-environmental and Soil Sciences, Guangdong Academy of Sciences, Guangzhou 510650, China
[b] School of Fisheries, Ludong University, Yantai 264025, China
[c] Center of Wastewater Resource Recovery, College of Resources and Environment, Fujian Agriculture and Forestry University, Fuzhou, Fujian 350002, China
[d] Geomicrobiology, Department of Geosciences, University of Tübingen 72076 Tübingen, Germany
[e] Cluster of Excellence: EXC 3121, TERRA – Terrestrial Geo-Biosphere Interactions in a Changing World, University of Tübingen 72076 Tübingen, Germany
[f] Cluster of Excellence: EXC 2124: Controlling Microbes to Fight Infection, 72074 Tübingen, Germany
[g] SCNU Environmental Research Institute, Guangdong Provincial Key Laboratory of Chemical Pollution and Environmental Safety & MOE Key Laboratory of Theoretical Chemistry of Environment, South China Normal University, Guangzhou 510006, China
[h] Institute of Surface-Earth System Science, School of Earth System Science, Tianjin University, Tianjin 300072, China

ARTICLE INFO

Associate Editor: H. Dong

Keywords:
Dissimilatory nitrate reduction to ammonium
Nitrite reduction
N and O isotope fractionation
NrfA
NirB

ABSTRACT

Dissimilatory nitrate reduction to ammonium (DNRA) is a major pathway of nitrogen (N) retention, yet its isotope systematics remain poorly constrained. Although DNRA and denitrification (DNF) share the same nitrate reductases, they diverge fundamentally at the nitrite reduction step, which represents the key biochemical distinction between N retention and N loss. Understanding N and oxygen (O) isotope fractionation during nitrite reduction is therefore critical for constraining isotopic signatures associated with DNRA pathways. This study systematically investigates dual N and O isotope fractionation associated with fermentative and respiratory DNRA pathways mediated by key nitrite reductases. Using pure-culture experiments spanning cytoplasmic (NirB) and periplasmic (NrfA-based) DNRA pathways, together with a mechanistic kinetic model, we demonstrate that different DNRA pathways generate characteristic and distinguishable N and O isotopic fingerprints. NirB-based fermentative DNRA showed a ratio of the O- and N-isotope effects (the $^{18}\varepsilon$:$^{15}\varepsilon$ ratio) of 0.45 ± 0.05, while NrfA-type respiratory DNRA exhibited a ratio of 1.15 ± 0.75. In contrast, multi-subunit NrfA-NrfH and NrfA-NrfB systems displayed negative $^{18}\varepsilon$:$^{15}\varepsilon$ ratios (−0.23 ± 0.30 and − 0.25 ± 0.09, respectively), indicating inverse O isotope fractionation linked to complex electron transfer mechanisms. These characteristic isotopic signatures provide a quantitative framework for identifying previously uncharacterized DNRA pathways in biogeochemical N cycling.

1. Introduction

Dissimilatory nitrate reduction to ammonium (DNRA) is a major anaerobic microbial pathway in the nitrogen (N) cycle that conserves reactive N as ammonium rather than releasing it as N_2 gas (Kaviraj et al., 2024). By retaining bioavailable N, DNRA directly competes with denitrification (DNF) and strongly influences ecosystem N availability, productivity, and nutrient loading (Cheng et al., 2022; Pan et al., 2023; Pandey et al., 2020). DNRA is increasingly recognized as an important N retention process in paddy soils, sediments, wetlands, and eutrophic aquatic systems (Cheng et al., 2022; Wei et al., 2022).

Despite its recognized ecological importance, the contribution of DNRA to N cycling in natural environments remains difficult to quantify. DNRA and DNF share similar nitrate reductases (Nar and Nap), while the nitrite reductases involved are fundamentally different (Stolz and Basu, 2002). As a result, the critical biochemical divergence between DNRA and DNF occurs at the nitrite reduction step (Pandey et al., 2020). While DNF reduces nitrite to N_2 gas via copper-containing (NirK) or

* Corresponding author.
E-mail address: txliu@soil.gd.cn (T. Liu).
[1] These authors contributed equally to this work.

https://doi.org/10.1016/j.gca.2026.11.008
Received 17 May 2026; Accepted 4 November 2026
Available online 11 November 2026
0016-7037/© 2026 Elsevier Ltd. All rights are reserved, including those for text and data mining, AI training, and similar technologies.

cytochrome cd1 (NirS) nitrite reductases, DNRA reduces nitrite directly to ammonium through distinct enzymatic pathways (Besson et al., 2022). DNRA comprises a fermentative pathway mediated by the cytoplasmic NADH-dependent nitrite reductase NirB and a respiratory pathway mediated by periplasmic cytochrome *c* nitrite reductases of the NrfA family (Chutivisut et al., 2024), including single-subunit NrfA systems and multi-subunit NrfA-NrfH and NrfA-NrfB complexes (Simon et al., 2000; Besson et al., 2022). This enzymatic divergence during nitrite reduction ultimately determines whether fixed N is retained within ecosystems or lost to the atmosphere (Cheng et al., 2022).

Dual natural-abundance isotope analysis of nitrate (δ^{15}N and δ^{18}O) provides a powerful, noninvasive tool for tracing microbial N transformations (Asamoto et al., 2021; Chen et al., 2023; Chen et al., 2024; Granger and Wankel, 2016). The proportionality of the O- and N-isotope effects (the $^{18}\varepsilon$:$^{15}\varepsilon$ ratio) of nitrate has successfully differentiated nitrate reduction pathways and enzyme systems, particularly Nar- versus Nap-mediated nitrate reduction processes (Asamoto et al., 2021; Chen et al., 2023; Chen et al., 2020; Frey et al., 2014; Granger et al., 2008; Margalef-Marti et al., 2026; Tischer et al., 2026; Treibergs and Granger, 2017; Visser et al., 2022). Enzyme-level studies have shown that membrane-bound Nar reductases produce nearly equal N and O isotope fractionation ($^{18}\varepsilon$:$^{15}\varepsilon \approx 1$) (Asamoto et al., 2021; Chen et al., 2023; Granger et al., 2008; Treibergs and Granger, 2017; Visser et al., 2022), whereas periplasmic Nap reductases impart lower ratios ($^{18}\varepsilon$:$^{15}\varepsilon \approx$ 0.4–0.7) (Chen et al., 2020; Frey et al., 2014; Granger et al., 2008; Treibergs and Granger, 2017). This isotope systematics has established a conceptual framework linking coupled N-O isotope fractionation to enzyme structure, electron-transfer pathways, and transport-related masking of intrinsic isotope effects.

In contrast to nitrate reduction, N and O isotope fractionation during nitrite reduction remains poorly constrained. N-O stable isotope studies of nitrite reduction have focused exclusively on DNF (Chen et al., 2023; Martin and Casciotti, 2016), while DNRA-specific nitrite reductases have received no investigation. Existing studies demonstrate that nitrite reduction during DNF produces enzyme-dependent isotopic signatures. For example, Martin and Casciotti (2016) reported distinct $^{18}\varepsilon$:$^{15}\varepsilon$ ratios for NirS- versus NirK-type nitrite reductases, whereas Chen et al. (2023) showed that chemical, microbial, and coupled nitrite reduction pathways yield markedly different isotope relationships. These results demonstrate that nitrite δ^{15}N-δ^{18}O signatures are sensitive to reaction mechanisms and electron-transfer pathways during DNF. Previous isotope studies further indicate that coupled N-O isotope effects can be strongly modified by nitrite transport limitations, highlighting the importance of distinguishing intrinsic from observed isotope effects during microbial nitrite reduction (Chen et al., 2023; Martin and Casciotti, 2016). The N and O isotope fractionation associated with DNRA nitrite reduction remains essentially unconstrained, preventing reliable interpretation of nitrite isotope signals in environments where DNRA and DNF coexist. Comparing fermentative NirB-mediated DNRA with respiratory pathways involving single-subunit NrfA and multi-subunit NrfA-NrfH and NrfA-NrfB pathways allows us to evaluate whether characteristic dual-isotopic signatures can differentiate DNRA-associated nitrite reduction pathways. Furthermore, by integrating isotope measurements with mechanistic kinetic modeling, this study further quantifies transport-related masking and constrains the intrinsic isotope effects associated with reductive N-O bond cleavage (Chen et al., 2023; Chen et al., 2020). This combined approach thus extends previous isotope studies from characterizing isotope fractionation during microbial nitrite reduction to mechanistically interpreting pathway-associated isotopic signatures and their underlying enzymatic controls during DNRA.

In this study, we address this fundamental gap through a systematic investigation of coupled N and O isotope fractionation during DNRA nitrite reduction. Four bacterial strains were selected to represent distinct DNRA nitrite-reduction systems with contrasting reductase architectures: the cytoplasmic NirB system in *Klebsiella pneumoniae* L17 and the periplasmic NrfA systems, including NrfA alone in *Shewanella oneidensis* MR-1, the NrfA-NrfB complex in *Shewanella putrefaciens* CN-32, and the NrfA-NrfH complex in *Geobacter metallireducens* GS-15. Using pure-culture experiments spanning fermentative and respiratory DNRA pathways, combined with a mechanistic kinetic model, we resolve isotopic signatures associated with cytoplasmic NirB and periplasmic NrfA-based systems. By integrating dual isotope measurements with kinetic modeling, we link distinct DNRA routes to characteristic N-O isotope patterns and establish a quantitative isotopic framework for identifying alternative DNRA pathways.

2. Materials and methods

2.1. Strains and bacterial cultivation

Four bacteria with the potential to dissimilate nitrite to ammonium were investigated, including *K. pneumoniae* L17 (Li et al., 2009), *S. oneidensis* MR-1 (Liu et al., 2020), *G. metallireducens* GS-15 (Liu et al., 2012), and *S. putrefaciens* CN-32 (Hu et al., 2020). *K. pneumoniae* L17 is a fermentative facultative bacterium, which was originally isolated from subterranean forest soil in Zhaoqing, China (Li et al., 2009). *S. oneidensis* MR-1 and *S. putrefaciens* CN-32 were purchased from MCCC (Marine Culture Collection of China, China) and the Guangdong Microbial Culture Collection Center (GDMCC), respectively. *G. metallireducens* GS-15 (ATCC 53774) was obtained from the laboratory culture collection of Derek R. Lovley, University of Massachusetts, Amherst, Massachusetts (Liu et al., 2012). *K. pneumoniae* L17, *S. oneidensis* MR-1, and *S. putrefaciens* CN-32 were revived in the LB medium containing 5 g L^{-1} NaCl, 5 g L^{-1} beef extract, and 10 g L^{-1} tryptone at pH 7.0. These strains were inoculated at 1% inoculum and then cultivated aerobically at 30℃ in the dark at 180 rpm. *G. metallireducens* GS-15 was resuscitated in FC medium with 20 mM acetate as the carbon source (Liu et al., 2012). The strain was cultured statically at 4% inoculum at 30℃ in the dark.

2.2. Batch experimental procedures

Anoxic batch experiments were conducted to quantify nitrite reduction kinetics and ammonium production. The anoxic medium included 30 mM PIPES, 10 mL/L trace element stock solution, 10 mL/L vitamins stock solution, 10 mM carbon source, and 3 mM sodium nitrite at pH 7.0, where trace elements and vitamins stock solution were replenished after autoclaving. The ingredients of trace elements and vitamins stock solution are provided in Tables S1 and S2. The carbon source for cultures of *S. oneidensis* MR-1 and *S. putrefaciens* CN-32 was sodium lactate. The carbon sources for cultures of *K. pneumoniae* L17 and *G. metallireducens* GS-15 were glucose and sodium acetate, respectively. A volume of 80 mL of medium was dispensed into 125 mL serum bottles and purged with N_2 gas by bubbling for 30 min to remove dissolved oxygen (Chen et al., 2020). The bottles were then sealed with butyl rubber plugs and aluminum caps, and autoclaved at 115°C for 20 min. The four strains were cultured to the logarithmic growth phase and were harvested by centrifuging at 8,000 × *g* for 5 min. The bacterial pellets were washed twice and resuspended in the sterilized anaerobic medium. Then, a 2.5% resuspension of each strain was inoculated into the corresponding sterilized anoxic medium. The treatment without cell inoculation was prepared as an abiotic control. All cultures were incubated at 30 ℃ in the dark, and duplicate cultures were destructively sampled at each time point.

N_2O concentrations were quantified using a gas chromatograph with an ECD detector (Techcomp GC7900, Tianmei, Shanghai, China) (Chen et al., 2023). Bacterial growth was monitored by measuring optical density at 600 nm (OD_{600}) using a UV–vis spectrophotometer (UV1102II, Techcomp Ltd., China). The concentrations of nitrite and nitrate in the samples were measured by ion chromatography (Dionex ICS-600, USA) with an anion exchange column (Dionex IonPac AS23 4 × 250 mm) (Chen et al., 2023). No nitrate was detected. The

concentrations of ammonium ions were detected by Nessler's reagent colorimetric method at 420 nm (Pan et al., 2023).

2.3. Experimental procedures for qPCR measuring of nitrite reductase genes

The cells of four strains, *K. pneumoniae* L17, *S. putrefaciens* CN-32, *S. oneidensis* MR-1, and *G. metallireducens* GS-15, were collected at the time of inoculation and in the logarithmic phase of nitrite conversion to ammonium under anaerobic conditions. Cells collected from duplicate cultures of each strain were pooled before RNA extraction. RNA was extracted using the AG RNAex Pro Reagent (Cat.# AG21101) following the manufacturer's instructions. Complementary DNA (cDNA) was synthesized from total RNA using the Evo M−MLV RT Kit with gDNA Clean for qPCR (Cat.# AG11711). Quantity of the synthesized cDNA was determined using Nanodrop ND-100 spectrophotometer. Primers specific for the nitrite reductase (cytochrome *c*-552) (*nrfA*), cytochrome *c* nitrite reductase small subunit (*nrfH*), pentaheme c-type cytochrome (*nrfB*), and nitrite reductase (NADH) large subunit (*nirB*) genes were designed and the internal reference primers were 16S-F/R from 16S rRNA conserved regions to target homologous genes of four strains (Table S3). To verify the specificity of the primers, PCR amplification of these genes was conducted. The DNA template (1 μL) was mixed with 12.5 μL of iTaq™ Universal SYBR® Green Supermix (2 ×), 1 μL primers (10 μM), and 9.5 μL RNase-free dH_2O. PCR reactions were initiated with denaturation at 94°C for 5 min, followed by 30 cycles of 94°C for 1 min, 60°C for 1 min, and 72°C for 1 min, with a final extension step of 72°C for 10 min. The PCR amplification products were determined by 1% agarose gel electrophoresis. Quantitative real-time polymerase chain reaction (qPCR) was carried out in three technical replicates under the following conditions: 1 μL forward primer, 1 μL reverse primer, 12.5 μL iTaq™ Universal SYBR® Green Supermix (2 ×), 9.5 μL RNase free dH_2O, and 1 μL cDNA. The qPCR conditions were as follows: an initial cycle of 94°C for 30 s; 35 cycles of 95°C for 5 s, 60°C for 30 s, followed by plate-reading step. Relative expression levels of the target genes were quantified using the $2^{-\triangle\triangle Ct}$ method based on qPCR fluorescence results.

2.4. Measurement of N and O isotopic compositions of nitrite

N and O isotopic compositions are reported in conventional δ notation (‰), where ($\delta^{15}N = [(^{15}N/^{14}N)_{sample} / (^{15}N/^{14}N)_{standard} - 1] \times 1000$ and $\delta^{18}O = [(^{18}O/^{16}O)_{sample} / (^{18}O/^{16}O)_{standard} - 1] \times 1000$). $R_{reactant}$ and $R_{product}$ refer to the isotope ratio of reactants and products, respectively. The magnitude of isotope fractionation between reactants and the products is quantified using the isotope fractionation factor α (where $\alpha = R_{reactant} / R_{product}$) or the corresponding enrichment factor ε (where $\varepsilon = (\alpha - 1) \times 1000$) (Mariotti et al., 1981). The values of $\delta^{15}N$ and $\delta^{18}O$ of the remaining nitrite were fitted to the Rayleigh fractionation equation to determine the α and ε values using Isoplot (version 4.15) (Chen et al., 2023). The $^{18}\varepsilon$:$^{15}\varepsilon$ ratio was determined from the slope of the linear regression between $\delta^{18}O$ and $\delta^{15}N$ using Isoplot (version 4.15), and its uncertainty was obtained from the corresponding regression output (Chen et al., 2023).

The $\delta^{15}N$ and $\delta^{18}O$ values of nitrite were analyzed using the bacterial approach (Sigman et al., 2001). In this procedure, *Pseudomonas chlororaphis* subsp. *aureofaciens* ATCC 13985, a denitrifying strain deficient in N_2O reductase activity, was employed to convert nitrite quantitatively into N_2O. The produced N_2O was subsequently introduced into an isoprime continuous flow isotope ratio mass spectrometer (CF-IRMS) equipped with a Gilson GX271 autosampler and a trace gas preconcentrator unit (IsoPrime, GV, UK) for isotope analysis. Calibration was performed using international reference materials (USGS-32, USGS-34, USGS-35, and IAEA-N3) and two laboratory reference materials. Analytical reproducibility, expressed as the standard deviation of replicate analyses for reference materials and samples was better than 0.3‰ for $\delta^{15}N$ and 0.5‰ for $\delta^{18}O$.

3. Results

3.1. Kinetics of DNRA

The nitrite reduction rates, expressed as first-order rate constants, displayed substantial variation among the four DNRA microorganisms, revealing distinct catalytic efficiencies. *K. pneumoniae* L17, which employs the cytoplasmic fermentative NirB enzyme, exhibited the most rapid nitrite consumption with a rate constant of 0.1583 h^{-1} ($R^2 = 0.93$) (Fig. 1a). In contrast, the respiratory-type DNRA bacteria exhibited comparatively slower reduction kinetics. The rate constant for *G. metallireducens* GS-15 (NrfA-NrfH system) was 0.0384 h^{-1} ($R^2 = 0.63$), followed by *S. oneidensis* MR-1 (NrfA) at 0.0227 h^{-1} ($R^2 = 0.96$). *S. putrefaciens* CN-32 (NrfA-NrfB system) showed the slowest nitrite reduction rate among the four tested strains, with a constant of 0.0057h^{-1} ($R^2 = 0.89$) (Fig. 1a). This hierarchy in reduction rates likely reflects differences in enzyme localization and associated nitrite transport challenges. The superior kinetic performance of *K. pneumoniae* L17 suggests a highly efficient intracellular nitrite reduction machinery and / or a highly efficient uptake of nitrite, albeit one that may be partially offset by the necessity for nitrite uptake across the cell membrane.

The kinetics of ammonium generation revealed a different pattern from nitrite reduction, highlighting variations in the efficiency of channeling reduced N to the final ammonium product (Fig. 1b). *K. pneumoniae* L17 and *G. metallireducens* GS-15 exhibited comparable and relatively high ammonium production rate constants of 0.0554 h^{-1} ($R^2 = 0.81$) and 0.0577 h^{-1} ($R^2 = 0.86$), respectively (Fig. 1b). A lower rate was observed for *S. oneidensis* MR-1 (0.0378h^{-1}, $R^2 = 0.82$), while *S. putrefaciens* CN-32 showed the slowest ammonium accumulation (0.0042 h^{-1}, $R^2 = 0.96$) (Fig. 1b). The disparity between the high nitrite reduction rate and the moderate ammonium production rate in *K. pneumoniae* L17 could indicate potential intermediate accumulation or alternative N fates within its fermentative metabolism. Alternatively, it is also possible that nitrite uptake into the cytoplasm is relatively rapid, resulting in fast apparent nitrite removal from the medium, whereas the subsequent enzymatic reduction steps leading to ammonium formation proceed more slowly and thus limit net ammonium accumulation. Conversely, the respiratory DNRA strains, particularly *G. metallireducens* GS-15, appear to couple nitrite reduction to ammonium release more directly.

Throughout the incubation period, none of the four strains produced detectable nitrous oxide (N_2O). Only ammonium (NH_4^+) accumulation was observed, and the consumption of nitrite (NO_2^-) was generally consistent with the increase in ammonium concentration, approximately maintaining an N balance (Fig. 1a and b). This observation indicates that the dominant N transformation in these cultures was DNRA rather than DNF. The absence of N_2O, a characteristic intermediate or byproduct of DNF, further suggests limited denitrifying activity in these systems.

3.2. Identification of genes encoding nitrite transformation

K. pneumoniae L17 is phylogenetically related to *K. pneumoniae* ATCC 13883^T (Li et al., 2009), with *nirB* identified as encoding the key enzyme for dissimilatory nitrite reduction to ammonium (Arivett et al., 2015). Gene amplification confirmed that *K. pneumoniae* L17 also contains the *nirB* gene (Fig. S1). Genome analysis revealed that *S. oneidensis* MR-1, *G. metallireducens* GS-15, and *S. putrefaciens* CN-32 contain the *nrfA* gene, which encodes a periplasmic nitrite reductase that catalyzes the conversion of nitrite to ammonium. In addition, *G. metallireducens* GS-15 and *S. putrefaciens* CN-32 possess the electron transfer subunits *nrfH* and *nrfB*, respectively (Figs. 2a and S1). NrfH mediates electron transport from menaquinol to NrfA. The two multiheme c-type cytochromes, NrfH and NrfA, form a membrane-bound complex that catalyzes menaquinol oxidation by nitrite during the respiratory nitrite ammonification in *G. metallireducens* GS-15 (Saghaï and Hallin, 2024). Additionally, NrfB, a

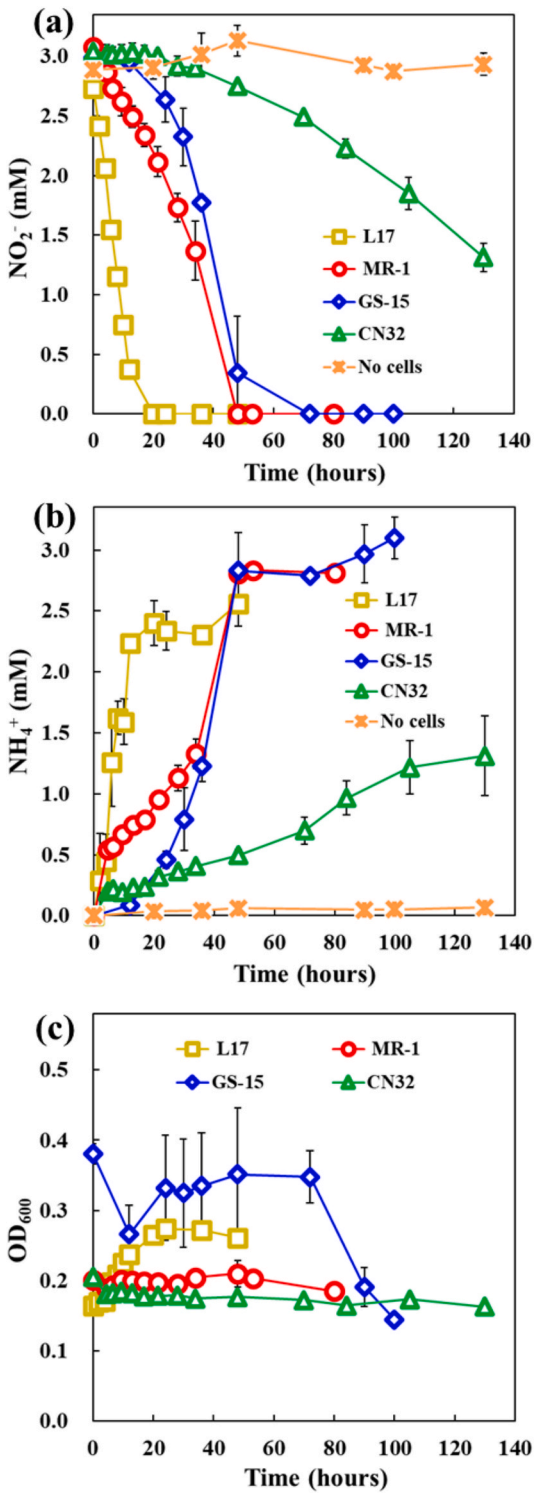

Fig. 1. (a) Time-dependent nitrite reduction by *K. pneumoniae* L17, *S. oneidensis* MR-1, *G. metallireducens* GS-15, and *S. putrefaciens* CN-32; (b) ammonium production during nitrite reduction by the same organisms; (c) changes in OD_{600} over the course of the incubation. OD_{600}, optical density measured at 600 nm, used as an indicator of cell density.

periplasmic pentaheme electron transfer cytochrome, is capable of transferring electrons to the catalytically competent NrfA in *S. putrefaciens* CN-32 (Edwards et al., 2020).

Fluorescence quantitative PCR analysis revealed distinct transcriptional responses of DNRA-related genes among the four strains (Fig. 2b). In *K. pneumoniae* L17, *nirB* expression was higher under anoxic conditions, consistent with the involvement of the NirB-mediated pathway in nitrite reduction to ammonium (Fig. 1b). Furthermore, a portion of the ammonium formed from dissimilated nitrite was incorporated into biomass through ammonium assimilation, promoting bacterial growth (Fig. 1c). Similarly, *nrfA* expression was increased in *S. oneidensis* MR-1 during incubation. In *G. metallireducens* GS-15, *nrfA* expression remained relatively low, whereas the electron-transfer gene nrfH showed higher expression, indicating distinct transcriptional responses of the catalytic and electron-transfer subunits. Notably, compared to other strains, *S. putrefaciens* CN-32 exhibited the highest expression levels of functional genes *nrfA* and *nrfB* (Fig. 2b), yet showed the slowest rate of ammonium production (Fig. 1b). This discrepancy indicates that transcript abundance alone does not necessarily reflect protein abundance or catalytic activity and cannot directly explain the observed differences in ammonium production. The high expression levels of *nrfA* and *nrfB* in *S. putrefaciens* CN-32 may reflect a transcriptional response under the cultivation conditions.

3.3. Dual N and O isotope fractionation during DNRA

The N enrichment factors ($^{15}\varepsilon$) during nitrite reduction differed among the four DNRA strains, reflecting the type of reductase involved. For the fermentative reductase NirB in *K. pneumoniae* L17, the $^{15}\varepsilon$ value was 4.5 ± 0.4‰ (Fig. 3a), indicating a N isotope fractionation associated with cytoplasmic nitrite reduction. *S. putrefaciens* CN-32, possessing the NrfA-NrfB complex, showed a $^{15}\varepsilon$ value similar to *K. pneumoniae* L17, at 5.4 ± 0.5‰ (Fig. 3a), suggesting comparable N isotope discrimination despite being a respiratory DNRA strain. In contrast, *G. metallireducens* GS-15 (NrfA-NrfH system) exhibited a significantly lower $^{15}\varepsilon$ value of 2.7 ± 0.5‰ (Fig. 3a), indicating reduced N isotope fractionation relative to *K. pneumoniae* L17 and *S. putrefaciens* CN-32. Finally, *S. oneidensis* MR-1 (NrfA) showed the lowest $^{15}\varepsilon$ value, 0.8 ± 0.6‰ (Fig. 3a), indicating minimal fractionation during nitrite reduction. O isotope enrichment factors ($^{18}\varepsilon$) also varied among strains (Fig. 3b). *K. pneumoniae* L17 and *S. oneidensis* MR-1 showed small positive $^{18}\varepsilon$ values of 2.0 ± 0.3‰ and 0.5 ± 1.0‰, respectively. In contrast, *S. putrefaciens* CN-32 and *G. metallireducens* GS-15 exhibited negative $^{18}\varepsilon$ values of − 1.5 ± 0.5‰ and − 0.7 ± 0.8‰, respectively (Fig. 3b).

The $^{18}\varepsilon$:$^{15}\varepsilon$ ratios were 0.45 ± 0.05 for *K. pneumoniae* L17, and 1.15 ± 0.75 for *S. oneidensis* MR-1. Negative $^{18}\varepsilon$:$^{15}\varepsilon$ ratios were therefore characteristic of the multi-subunit NrfA-NrfH and NrfA-NrfB systems, with values of − 0.23 ± 0.30 for *G. metallireducens* GS-15, and − 0.25 ± 0.09 for *S. putrefaciens* CN-32 (Fig. 3c; Table 1).

4. Discussion

4.1. DNRA nitrite reduction exhibits pathway-associated isotope systematics

The differences in observed isotope enrichment factors among DNRA strains were not proportional to the differences in nitrite reduction rates, indicating that the observed isotopic signatures cannot be explained by overall reaction kinetics. Instead, they may reflect the combined effects of two primary factors: (i) intrinsic isotope effects associated with the catalytic N-O bond cleavage step, and (ii) masking effects imposed by nitrite transport (Chen et al., 2023; Martin and Casciotti, 2016). Differences among DNRA reductase systems may influence both factors. Additionally, differences in electron supply, substrate accessibility, and cellular physiology may influence mass-transfer limitation, thereby affecting the observed N and O isotope fractionation (Chen et al., 2024; Margalef-Marti et al., 2026).

In *S. oneidensis* MR-1, the very small $^{15}\varepsilon$ value suggests strong suppression of isotope fractionation (Fig. 3a). This fractionation is consistent with a mass-transfer or binding limitation during periplasmic nitrite reduction, which can substantially dampen the observable isotope effect even when the intrinsic enzymatic discrimination is large (Chen et al.,

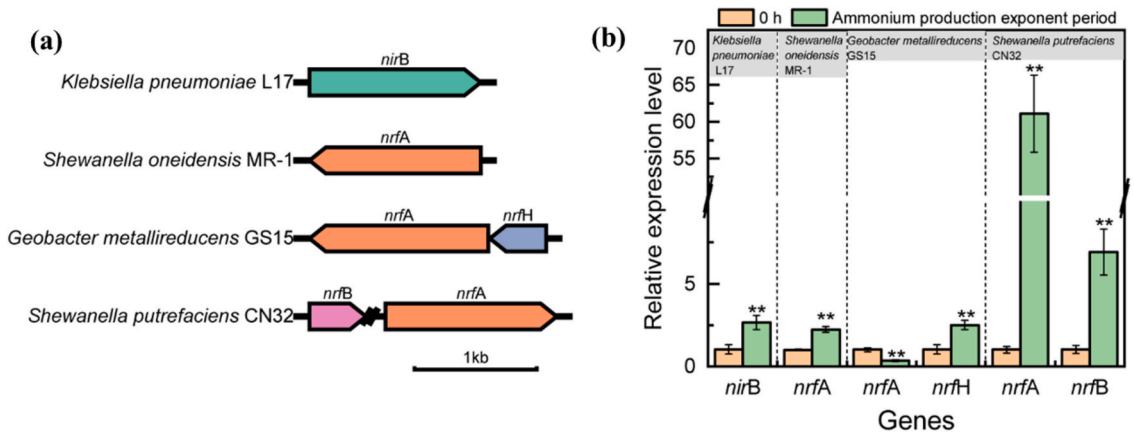

Fig. 2. Annotated dissimilatory nitrite to ammonium genes (a) and relative expression levels (b) in *K. pneumoniae* L17, *S. oneidensis* MR-1, *G. metallireducens* GS-15, and *S. putrefaciens* CN-32. Error bars indicate standard deviations of three technical replicates. $^{**}P < 0.01$ as determined using analysis of variance (ANOVA).

2024). Processes such as diffusion across the outer membrane and transient binding of nitrite to the enzyme active site may reduce the expression of N isotope fractionation in the residual nitrite pool (Kritee et al., 2012). In contrast, *K. pneumoniae* L17, which employs the cytoplasmic NirB enzyme, exhibits a larger $^{15}\varepsilon$ value, indicating that intracellular nitrite reduction may allow greater expression of the underlying isotope effect. This comparison highlights that differences in observed N isotope fractionation do not necessarily imply differences in the chemical step of nitrite reduction, but instead reflect variability in how strongly that step is masked by upstream processes (Buchwald et al., 2016; Chen et al., 2023).

The O enrichment factor ($^{18}\varepsilon$) for *K. pneumoniae* L17 (NirB) of 2.0 ± 0.3‰ is substantially smaller than the corresponding $^{15}\varepsilon$ value (Fig. 3b). *S. oneidensis* MR-1 (NrfA) exhibited a lower O isotope fractionation of 0.5 ± 1.0‰ (Fig. 3b), indicating that the intrinsic O isotope effect associated with nitrite reduction is largely masked at the system level. This suppression is most plausibly attributed to transport-related masking during periplasmic nitrite reduction, where rapid substrate exchange and diffusional processes may limit the expression of intrinsic O isotope discrimination (Martin and Casciotti, 2016). Under such conditions, the rate-limiting steps occur upstream of N-O bond cleavage, thereby limiting the expression of the intrinsic O isotope effect (Chen et al., 2024). In contrast, *S. putrefaciens* CN-32 (NrfA-NrfB complex) and *G. metallireducens* GS-15 (NrfA-NrfH system) displayed distinct and opposite ^{18}O fractionation patterns. These inverse or reduced O isotope effects are likely linked to the presence of multi-heme electron transfer complexes, which introduce additional reaction steps and may promote partial O atom exchange between nitrite and water during reduction (Martin and Casciotti, 2016; Visser et al., 2022). The direction and magnitude of O isotope fractionation therefore appear to be governed not only by the catalytic NrfA subunit itself, but also by the architecture of associated electron transfer modules. Although inverse isotope effects have also been reported during microbial nitrite oxidation (Casciotti, 2009), that study reported an inverse N isotope effect, with residual nitrite becoming progressively depleted in ^{15}N as the reaction proceeded, rather than an inverse O isotope effect. In contrast, the present study observed normal N isotope fractionation.

4.2. $^{18}\varepsilon$:$^{15}\varepsilon$ ratios in fermentative and respiratory DNRA

The observed $^{18}\varepsilon$:$^{15}\varepsilon$ ratios provide a promising isotopic indicator for differentiating between the fermentative and respiratory DNRA pathways, as well as distinguishing among specific nitrite reductase types. The distinct $^{18}\varepsilon$:$^{15}\varepsilon$ ratio for K. pneumoniae L17 is characteristic of the fermentative pathway catalyzed by the cytoplasmic NADH-dependent NirB enzyme (Fig. 3c). This fermentative process occurs entirely within the cytoplasm (Arshad et al., 2017). The reliance on intracellular water as the O source for the nitrite O atoms, combined with potential kinetic limitations imposed by nitrite transport across the cell membrane, dampens the expression of O isotope fractionation relative to N, resulting in a lower $^{18}\varepsilon$:$^{15}\varepsilon$ ratio.

In contrast, the respiratory pathway mediated by the periplasmic NrfA enzyme for S. oneidensis MR-1 was associated with a markedly higher $^{18}\varepsilon$:$^{15}\varepsilon$ ratio (Fig. 3c). In this system, as exemplified by S. oneidensis MR-1 which lacks NrfH and relies directly on CymA for electrons, the catalytic subunit NrfA is situated in the periplasm, allowing direct and rapid access to extracellular nitrite (Gao et al., 2009). This periplasmic localization may facilitate a more complete expression of the intrinsic O isotope effect of the NrfA enzyme itself, potentially contributing to a high $^{18}\varepsilon$:$^{15}\varepsilon$ ratio.

The strongly negative $^{18}\varepsilon$:$^{15}\varepsilon$ ratios observed for G. metallireducens GS-15 and S. putrefaciens CN-32 represent distinct isotope patterns associated with the multi-subunit respiratory nitrite reductases systems (NrfA-NrfH and NrfA-NrfB, respectively) (Fig. 3c). The NrfA-NrfH complex in *G. metallireducens* involves a dedicated membrane-bound tetraheme cytochrome *c* (NrfH) that shuttles electrons from the quinone pool directly to the catalytic NrfA subunit (Simon et al., 2000). Similarly, the NrfA-NrfB system in S. putrefaciens CN-32 represents a variant of the multi-subunit NrfABCD complex (Hussain et al., 1994). In both cases, the presence of dedicated electron transfer modules (NrfH or NrfB) that form tight complexes with NrfA likely alters electron-transfer dynamics during nitrite reduction (Besson et al., 2022). The intricate, multi-step electron transfer through the heme networks in these complexes, potentially coupled with O atom exchange between reaction intermediates and water molecules at the active site of NrfA, may contribute to the inverse fractionation effect for O isotopes, thereby producing the characteristic negative $^{18}\varepsilon$:$^{15}\varepsilon$ ratios. The remarkable similarity between the ratios for *G. metallireducens* GS-15 and S. putrefaciens CN-32, despite their different electron-transfer modules (NrfH vs. NrfB), suggests that the isotope behavior may reflect a shared mechanistic feature associated with the NrfA catalytic subunit when operating within multi-subunit complexes (Besson et al., 2022; Einsle et al., 2002). The distinct isotopic signatures observed among fermentative and respiratory DNRA pathways further indicate that nitrite isotope measurements may help identify dominant reductase architectures active in the environment (Fig. 6).

The $^{18}\varepsilon$:$^{15}\varepsilon$ ratios associated with all DNRA pathways show distinct values from those reported for DNF, where NirS- and NirK-mediated nitrite reduction typically yields ratios of 0.75 and 0.09, respectively (Martin and Casciotti, 2016). This contrast likely reflects differences in electron flow and catalytic mechanisms between the two processes, as DNRA channels electrons toward ammonium production, whereas DNF

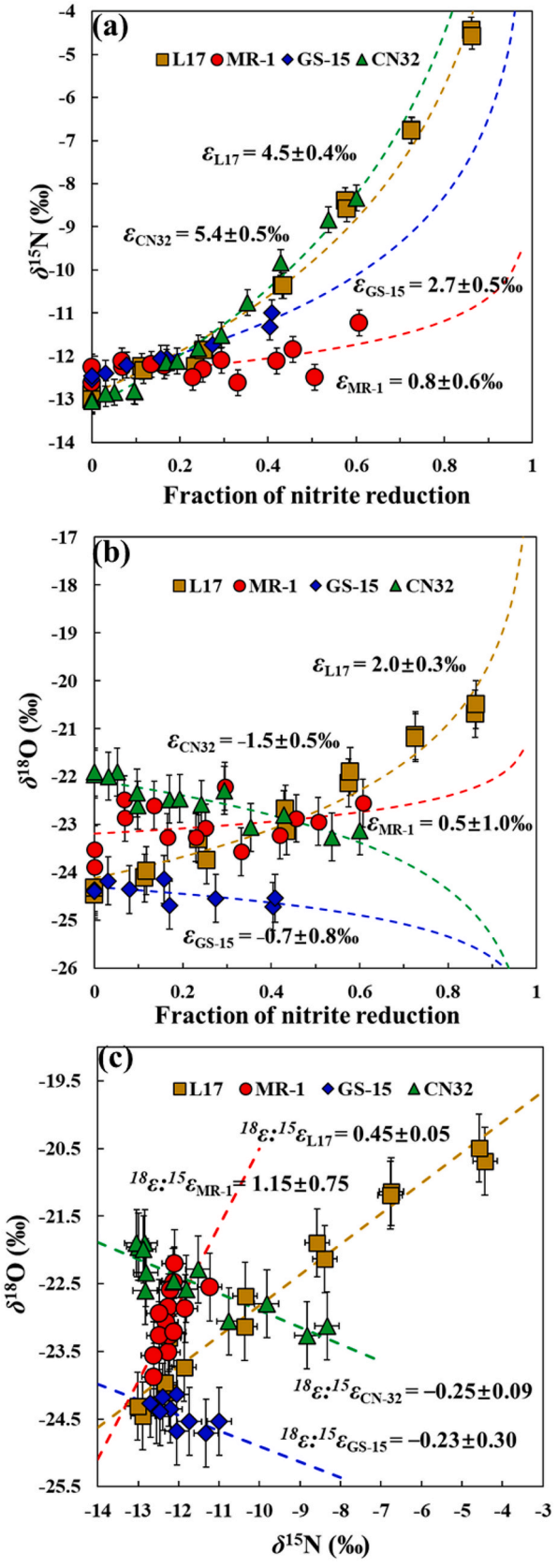

Fig. 3. (a) N isotopic composition (δ^{15}N) vs. fraction of nitrite reduction; (b) O isotopic composition (δ^{18}O) vs. fraction of nitrite reduction; and (c) the relationship between δ^{18}O and δ^{15}N, with the slope representing the $^{18}\varepsilon$:$^{15}\varepsilon$ ratio during nitrite reduction by *K. pneumoniae* L17, *S. oneidensis* MR-1, *G. metallireducens* GS-15, and *S. putrefaciens* CN-32.

Table 1
Dual N and O isotope enrichment factors, and the ratios of $^{18}\varepsilon$:$^{15}\varepsilon$ during dissimilatory nitrite reduction to ammonium by different strains.

Strains	Reductase	$^{15}\varepsilon$ (‰)	$^{18}\varepsilon$ (‰)	$^{18}\varepsilon$:$^{15}\varepsilon$
K. pneumoniae L17	NirB	4.5 ± 0.4	2.0 ± 0.3	0.45 ± 0.05
S. oneidensis MR-1	NrfA	0.8 ± 0.6	0.5 ± 1.0	1.15 ± 0.75
G. metallireducens GS-15	NrfA-NrfH	2.7 ± 0.5	–0.7 ± 0.8	–0.23 ± 0.30
S. putrefaciens CN-32	NrfA-NrfB	5.4 ± 0.5	–1.5 ± 0.5	–0.25 ± 0.09

partitions electrons among gaseous intermediates and products (NO, N_2O, and N_2) (Pan et al., 2023). These differences provide a basis for exploring the isotopic distinction between N retention and N loss.

4.3. Quantifying mass-transfer masking and intrinsic isotope effects during DNRA using a kinetic framework

To disentangle intrinsic enzymatic isotope effects from transport-related masking during DNRA, we applied a kinetic model that explicitly resolves elementary reaction steps associated with nitrite reduction. The DNRA process was conceptualized as a sequence of three reactions (Table 2): (R1) reduction of the oxidized nitrite reductase ($Enzyme_{ox}$) to its reduced form ($Enzyme_{red}$); (R2) diffusion and binding of nitrite to $Enzyme_{red}$, forming an $Enzyme_{red}{\cdot}NO_2^-$ complex; and (R3) cleavage of the N-O bond and subsequent reduction of nitrite to ammonium, accompanied by regeneration of $Enzyme_{ox}$. k_1, k_2^+, k_2^-, and k_3 represent rate constants of R1- R3 (Table 2; Table 3). Through fitting the experimental data observed in Fig. 1a and b using the kinetic model, the rate constants of the individual elementary reactions involved in nitrite reduction were obtained (Figs. 4 and 5). The uncertainty of the fitted rate constants was evaluated from the Chi^2/Min Chi^2 profiles, with a threshold of 0.95 used to determine the upper and lower bounds (Fig. 5; Table 3). Within this framework, the relationship between the observed kinetic isotope effect (α_{AKIE}) and the intrinsic isotope effect associated with N-O bond cleavage (α_{KIE}) can be expressed as (Chen et al. 2020; Treibergs and Granger, 2017):

$$\alpha_{AKIE} = \frac{\alpha_{KIE} + C}{1 + C} \quad (1)$$

where C represents a partitioning coefficient, which is equal to k_3/k_2^-, with k_3 and k_2^- obtained from the kinetic model. The value of α_{KIE} was then calculated from Eq. (1) using the measured α_{AKIE} and the model-derived C value. Within the kinetic model, C describes the relative rates of the N-O bond cleavage step and the reverse substrate-binding step, providing a model-based indication of the extent to which mass-transfer limitations affect the expression of the intrinsic isotope effect. Large C values indicate strong mass-transfer control, leading to pronounced suppression of observable isotope fractionation, whereas small

Table 2
Elementary reactions included in the kinetic model for dissimilatory nitrite reduction to ammonium.

No.	Reactions
R1	$ED + Enzyme_{ox} \xrightarrow{k_1} EP + Enzyme_{red}$
R2	$NO_2^- + Enzyme_{red} \underset{k_2^-}{\overset{k_2^+}{\rightleftharpoons}} Enzyme_{red} \bullet NO_2^-$
R3	$Enzyme_{red} \bullet NO_2^- \xrightarrow{k_3} NH_4^+ + Enzyme_{ox}$

ED denotes the electron donor. Sodium lactate was used as the electron donor for cultures of *S. oneidensis* MR-1 and *S. putrefaciens* CN-32, whereas glucose and sodium acetate were used as the electron donors for cultures of *K. pneumoniae* L17 and *G. metallireducens* GS-15, respectively. EP denotes the oxidation product of the electron donor. $Enzyme_{red}$ and $Enzyme_{ox}$ represent the reduced and oxidized forms of the nitrite reductase, which are NirB for *K. pneumoniae* L17, NrfA for *S. oneidensis* MR-1, NrfA-NrfH for *G. metallireducens* GS-15, and NrfA-NrfB for *S. putrefaciens* CN-32, respectively.

Table 3
Kinetic model-derived rate constants and *C* values during dissimilatory nitrite reduction to ammonium.

Strains	*k*	Best-fit value	Lower bound	Upper bound	C
K. pneumoniae L17	k_1	0.053	0.010	0.90	11.14
	k_2^+	0.056	0.046	0.071	
	k_2^-	0.14	0.023	1.35	
	k_3	1.56	0.76	9.9	
S. oneidensis MR-1	k_1	0.016	0.0064	0.26	60.81
	k_2^+	0.012	0.0105	0.0138	
	k_2^-	0.037	5.3×10^{-6}	0.39	
	k_3	2.25	1.4	23.7	
G. metallireducens GS-15	k_1	0.0061	6.1×10^{-7}	0.10	17.37
	k_2^+	0.0064	0.0038	0.011	
	k_2^-	0.20	0.0035	3.3	
	k_3	3.4	2.7	14.8	
S. putrefaciens CN-32	k_1	0.0034	2.8×10^{-5}	0.16	8.13
	k_2^+	0.0026	0.0021	0.0034	
	k_2^-	0.16	0.044	0.66	
	k_3	1.3	0.086	32.2	

C values allow more complete expression of the intrinsic fractionation.

Model-derived *C* values varied substantially among the four DNRA microorganisms investigated (Table 3), ranging from 8.13 for *S. putrefaciens* CN-32 (NrfA-NrfB system) to 60.81 for *S. oneidensis* MR-1 (NrfA). These differences indicate marked variability in the degree of transport and binding limitation among DNRA pathways, consistent with differences in enzyme localization (cytoplasmic versus periplasmic), electron-transfer architecture, and substrate accessibility. The kinetic model yields similar intrinsic N isotope fractionation factors ($^{15}\varepsilon_{intrinsic}$) associated with reductive N-O bond cleavage across all respiratory NrfA-based systems, which range from 49.3 to 49.6‰ and include NrfA alone, NrfA-NrfH, and NrfA-NrfB. The inferred $^{15}\varepsilon_{intrinsic}$ is slightly higher for the fermentative NirB pathway in *K. pneumoniae* L17 (54.6‰) than for the respiratory NrfA-based systems (Table 3). These $^{15}\varepsilon_{intrinsic}$ values are comparable to previously reported model-derived intrinsic isotope enrichment factors for other reductive N-O bond cleavage processes. The model-derived $^{15}\varepsilon_{intrinsic}$ associated with Fe(II)-driven nitrite reduction was estimated to be approximately 52‰ (Chen et al. 2021), which is similar to the values obtained for biological nitrite reduction in this study.

The close similarity of intrinsic isotope effects among NirB and NrfA-based pathways contrasts sharply with their highly divergent observed fractionation factors and supports an important role for mass-transfer masking in shaping observed isotopic signatures. In particular, the very large model-derived *C* value for *S. oneidensis* MR-1 suggests substantial diffusion and binding limitations within the modeled NrfA system, potentially suppressing the expression of a large intrinsic isotope effect. Conversely, the lower *C* value for NirB reflects weaker nitrite transport limitation, allowing a greater fraction of the intrinsic isotope effect to be expressed in the residual nitrite pool. Overall, integrating dual N-O isotope measurements with a mechanistic kinetic model provides a quantitative basis for distinguishing intrinsic enzymatic isotope effects from extrinsic masking processes during DNRA.

4.4. Environmental implications

Distinguishing respiratory pathways from fermentative pathways remains a major challenge in natural and engineered systems (e.g., paddy soils, wetlands). The observed variability in $^{18}\varepsilon$:$^{15}\varepsilon$ ratios among NirB-, NrfA-, NrfA-NrfH-, and NrfA-NrfB-mediated pathways highlights the sensitivity of N and O isotope fractionation to reductase architecture and electron-transfer mechanisms. This contrasting N and O isotope fractionation provides mechanistic insights into DNRA-associated nitrite reduction.

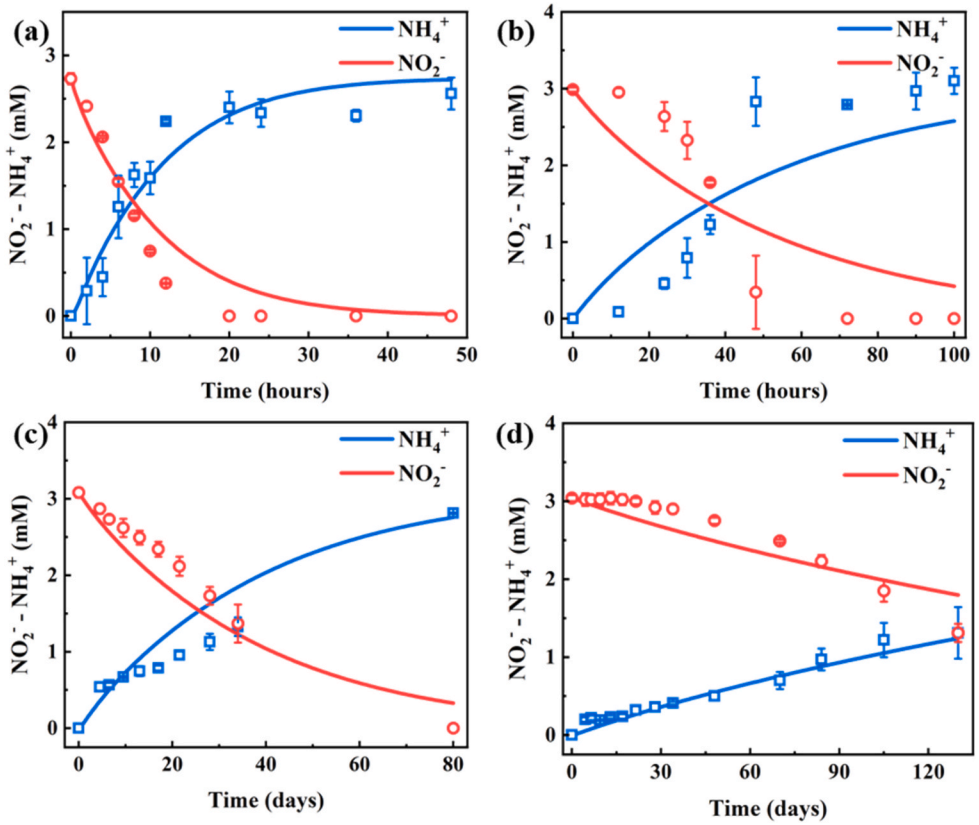

Fig. 4. Kinetic model-fitted concentrations of nitrite and ammonium during nitrite reduction by *K. pneumoniae* L17 (a), *S. oneidensis* MR-1 (b), *G. metallireducens* GS-15 (c), and *S. putrefaciens* CN-32 (d).

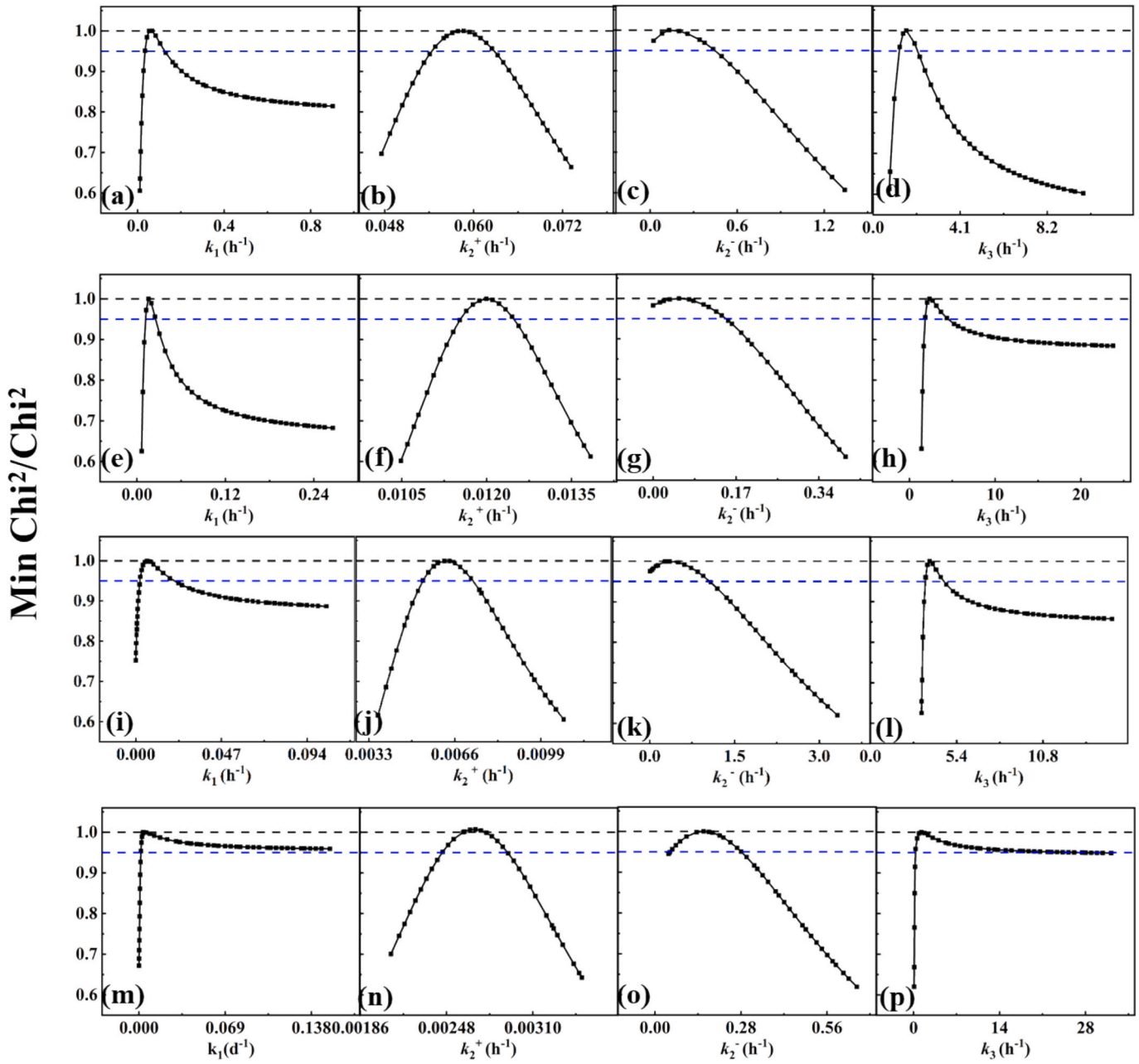

Fig. 5. The plot of Chi^2/Min Chi^2 as a function of the rate constant *k*. Upper and lower limits of *k* were obtained using a threshold of 0.95. Panels (a-d) show results for nitrite reduction by *K. pneumoniae* L17, (e)-(h) correspond to nitrite reduction by *S. oneidensis* MR-1, (i)-(l) correspond to nitrite reduction by *G. metallireducens* GS-15, and (m)-(p) correspond to nitrite reduction by *S. putrefaciens* CN-32.

Understanding the isotope systematics associated with DNRA nitrite reduction has important implications for interpreting biogeochemical N cycling. Although DNRA and DNF share the same nitrate reductases, they diverge at the nitrite reduction step through distinct nitrite reductases and electron-transfer architectures. This biochemical divergence makes nitrite reduction a critical step controlling isotopic differentiation between N retention and N loss pathways. The differences between DNRA and previously reported DNF isotope relationships suggest that coupled N-O isotope analysis of nitrite may help constrain the relative contributions of these processes in environments where they coexist. However, given the limited isotope dataset currently available for both DNRA and DNF during microbial nitrite reduction and the uncertainty associated with some $^{18}\varepsilon$:$^{15}\varepsilon$ ratios, these isotopic relationships should be interpreted as a promising constraint rather than universal quantitative endmembers for environmental DNRA and DNF. Furthermore, the coexistence of multiple N transformation processes in natural environments (e.g., anammox, assimilation, and N recycling), may complicate the interpretation of N and O isotopic signatures (Chen et al., 2024; Margalef-Marti et al., 2026; Wang et al., 2024). Coupling isotope measurements with mechanistic kinetic modeling therefore provides a quantitative basis for separating intrinsic enzymatic isotope effects from transport-related masking processes, improving interpretation of isotopic signatures under environmentally relevant conditions.

In this study, *K. pneumoniae* L17, *S. oneidensis* MR-1, *G. metallireducens* GS-15, and *S. putrefaciens* CN-32 were used as DNRA model bacteria. However, DNRA can be performed by many widespread bacteria in natural environments, indicating that the isotope systematics identified here may extend beyond the specific strains investigated in this study. Moreover, nitrite can transiently accumulate under conditions where nitrate reduction to nitrite exceeds subsequent nitrite

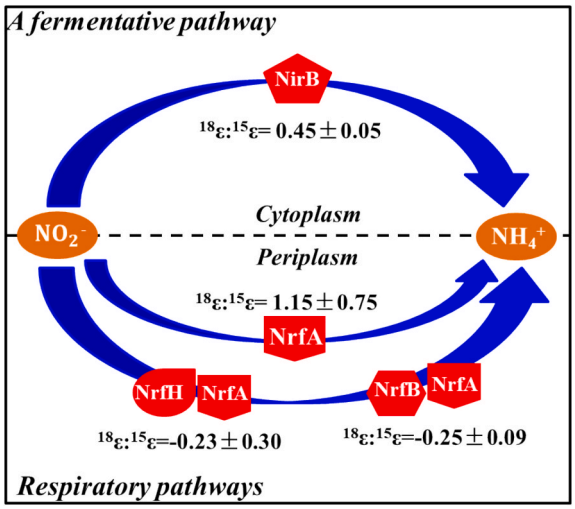

Fig. 6. Conceptual model illustrating distinct dissimilatory nitrite reduction to ammonium pathways and their characteristic dual N and O isotope fractionation signatures.

reduction, particularly under high nitrate loading or when the downstream reduction step is relatively limited. Nevertheless, further investigation under lower nitrite concentrations would still be valuable, as lower nitrite concentrations may alter the relative importance of nitrite transport and consequently affect the expression of observed isotope effects. Therefore, while the isotope framework developed here provides a potential basis for interpreting DNRA pathways, its applicability to complex environmental systems, including a broader range of bacterial strains, as well as varying nitrite concentrations and electron donor availability requires further investigation.

5. Conclusions

This study systematically characterized coupled N and O isotope fractionation during nitrite reduction across distinct DNRA pathways. Fermentative and respiratory DNRA pathways produced characteristic and distinguishable isotopic signatures linked to nitrite reductase architecture and electron-transfer mechanisms. NirB-mediated fermentative DNRA exhibited an $^{18}\varepsilon$:$^{15}\varepsilon$ ratio of 0.45 ± 0.05, whereas single-subunit NrfA-mediated respiratory DNRA showed a ratio of 1.15 ± 0.75. In contrast, multi-subunit NrfA-NrfH and NrfA-NrfB systems generated inverse O isotope fractionation, producing negative $^{18}\varepsilon$:$^{15}\varepsilon$ ratios of − 0.23 ± 0.30 and − 0.25 ± 0.09, respectively. These findings highlight the importance of nitrite transport, enzyme accessibility, and electron-transfer architecture in controlling the expression of isotope fractionation during DNRA. By integrating dual N and O isotope measurements with kinetic modeling, this study provides evidence for distinct isotopic patterns associated with the four DNRA systems investigated and establishes a mechanistic basis for using these isotopic patterns to distinguish DNRA pathways and to interpret the fate of reactive N in natural and engineered environments.

Data availability

Data are available through Mendeley Data at https://data.mendeley.com/datasets/c8xtymvwkt/1.

CRediT authorship contribution statement

Guojun Chen: Writing – original draft, Methodology, Investigation, Formal analysis. **Qinqin Hao:** Writing – review & editing, Methodology, Investigation. **Yan Ru:** Visualization. **Andreas Kappler:** Writing – review & editing. **Raymond Jianxiong Zeng:** Writing – review & editing. **Xiaomin Li:** Writing – review & editing. **Zebin Hong:** Investigation. **Fanghua Liu:** Formal analysis. **Fujun Yue:** Methodology. **Shiwen Hu:** Writing – review & editing. **Tongxu Liu:** Writing – review & editing, Supervision, Funding acquisition, Conceptualization.

Declaration of competing interest

The authors declare that they have no known competing financial interests or personal relationships that could have appeared to influence the work reported in this paper.

Acknowledgments

This work was funded by National Natural Science Foundation of China (42125704, 42677037, 42577141), National Key R&D Program of China (2023YFC3706902), Basic and Applied Basic Research Foundation of Guangdong (2026A1515010685), Youth S&T Talent Support Program of GDSTA (SKXRC2025097), Young Talent Support Project of Guangzhou Association for Science and Technology (QT-2025-022), and Guangdong Foundation for Program of Science and Technology Research (2023B1212060044).

Appendix A. Supplementary material

Supplementary material to this article can be found online at https://doi.org/10.1016/j.gca.2026.11.008.

The supplementary material comprises the following items: Components of trace element stock solution (Table S1); components of vitamins stock solution (Table S2); primer pairs for quantitative real-time polymerase chain reaction (qPCR) for nitrite reductase (cytochrome *c*-552) (*nrfA*) and nitrite reductase (NADH) large subunit (*nirB*) and electron carriers (*nrfH* and *nrfB*) genes (Table S3); agarose gel electrophoresis of nitrite reductase (cytochrome *c*-552) (*nrfA*) and nitrite reductase (NADH) large subunit (*nirB*) and electron carriers (*nrfH* and *nrfB*) genes fragments generated in PCR reactions using cDNA as template (Fig. S1).

References

Arivett, B.A., Ream, D.C., Fiester, S.E., Mende, K., Murray, C.K., Thompson, M.G., Kanduru, S., Summers, A.M., Roth, A.L., Zurawski, D.V., Actis, L.A., 2015. Draft genome sequences of *Klebsiella pneumoniae* clinical type strain ATCC 13883 and three multidrug-resistant clinical isolates. Genome Announc. 3.

Arshad, A., Dalcin Martins, P., Frank, J., Jetten, M.S.M., Op den Camp, H.J.M., Welte, C. U., 2017. Mimicking microbial interactions under nitrate-reducing conditions in an anoxic bioreactor: enrichment of novel *Nitrospirae* bacteria distantly related to *Thermodesulfovibrio*. Environ. Microbiol. 19, 4965–4977.

Asamoto, C.K., Rempfert, K.R., Luu, V.H., Younkin, A.D., Kopf, S.H., 2021. Enzyme-specific coupling of oxygen and nitrogen isotope fractionation of the *nap* and *nar* nitrate reductases. Environ. Sci. Technol. 55, 5537–5546.

Besson, S., Almeida, M.G., Silveira, C.M., 2022. Nitrite reduction in bacteria: a comprehensive view of nitrite reductases. Coord. Chem. Rev. 464, 214560.

Buchwald, C., Grabb, K., Hansel, C.M., Wankel, S.D., 2016. Constraining the role of iron in environmental nitrogen transformations: dual stable isotope systematics of abiotic NO_2^- reduction by Fe(II) and its production of N_2O. Geochim. Cosmochim. Acta 186, 1–12.

Casciotti, K.L., 2009. Inverse kinetic isotope fractionation during bacterial nitrite oxidation. Geochim. Cosmochim. Acta 73 (7), 2061–2076.

Chen, D., Cheng, K., Liu, T., Chen, G., Kappler, A., Li, X., Zeng, R.J., Yang, Y., Yue, F., Hu, S., Cao, F., Li, F., 2023. Novel insight into microbially mediated nitrate-reducing Fe(II) oxidation by *Acidovorax* sp. strain BoFeN1 using dual N-O isotope fractionation. Environ. Sci. Technol. 57, 12546–12555.

Chen, G., Chen, D., Li, F., Liu, T., Zhao, Z., Cao, F., 2020. Dual nitrogen-oxygen isotopic analysis and kinetic model for enzymatic nitrate reduction coupled with Fe(II) oxidation by *Pseudogulbenkiania* sp. strain 2002. Chem. Geol. 534, 119456.

Chen, G., Hao, Q., Zeng, R.J., Kappler, A., Li, X., Yue, F., Hu, S., Yang, Y., Liu, F., Li, H., Qian, D., Yang, B., Sarkytkan, K., Liu, T., Li, F., 2024. Unraveling the mechanism of assimilatory nitrate reduction and methane oxidation by *Methylobacter* sp. YHQ through dual N-O isotope analysis and kinetic modeling. Carbon Res. 3, 58.

Chen, G., Zhao, W., Yang, Y., Chen, D., Wang, Y., Li, F., Zhao, Z., Cao, F., Liu, T., 2021. Chemodenitrification by Fe(II) and nitrite: effects of temperature and dual N-O isotope fractionation. Chem. Geol. 575, 120258.

Cheng, Y., Elrys, A.S., Merwad, A.-R.-M., Zhang, H., Chen, Z., Zhang, J., Cai, Z., Müller, C., 2022. Global patterns and drivers of soil dissimilatory nitrate reduction to ammonium. Environ. Sci. Technol. 56, 3791–3800.

Chutivisut, P., Rison, K., Mhuantong, W., Faiyue, B., 2024. Occurrence of fermentative and respiratory dissimilatory nitrate reduction to ammonium (DNRA) in flooded rice soil ecosystems: potential pathways for nitrogen fertilizer management through organic supplementation. Case Stud. Chem. Environ. Eng. 10, 100980.

Edwards, M.J., White, G.F., Butt, J.N., Richardson, D.J., Clarke, T.A., 2020. The crystal structure of a biological insulated transmembrane molecular wire. Cell 181, 665–673.e610.

Einsle, O., Messerschmidt, A., Huber, R., Kroneck, P.M.H., Neese, F., 2002. Mechanism of the six-electron reduction of nitrite to ammonia by cytochrome *c* nitrite reductase. J. Am. Chem. Soc. 124, 11737–11745.

Frey, C., Hietanen, S., Jürgens, K., Labrenz, M., Voss, M., 2014. N and O isotope fractionation in nitrate during chemolithoautotrophic denitrification by *sulfurimonas gotlandica*. Environ. Sci. Technol. 48, 13229–13237.

Gao, H., Yang, Z.K., Barua, S., Reed, S.B., Romine, M.F., Nealson, K.H., Fredrickson, J.K., Tiedje, J.M., Zhou, J., 2009. Reduction of nitrate in *Shewanella oneidensis* depends on atypical NAP and NRF systems with NapB as a preferred electron transport protein from CymA to NapA. ISME J. 3, 966–976.

Granger, J., Sigman, D.M., Lehmann, M.F., Tortell, P.D., 2008. Nitrogen and oxygen isotope fractionation during dissimilatory nitrate reduction by denitrifying bacteria. Limnol. Oceanogr. 53, 2533–2545.

Granger, J., Wankel, S.D., 2016. Isotopic overprinting of nitrification on denitrification as a ubiquitous and unifying feature of environmental nitrogen cycling. Proc. Natl. Acad. Sci. USA 113, E6391–E6400.

Hu, S., Wu, Y., Ding, Z., Shi, Z., Li, F., Liu, T., 2020. Facet-dependent reductive dissolution of hematite nanoparticles by *Shewanella putrefaciens* CN-32. Environ. Sci. Nano 7, 2522–2531.

Hussain, H., Grove, J., Griffiths, L., Busby, S., Cole, J., 1994. A seven-gene operon essential for formate-dependent nitrite reduction to ammonia by enteric bacteria. Mol. Microbiol. 12, 153–163.

Kaviraj, M., Kumar, U., Chatterjee, S., Parija, S., Padbhushan, R., Nayak, A.K., Gupta, V. V.S.R., 2024. Dissimilatory nitrate reduction to ammonium (DNRA): a unique biogeochemical cycle to improve nitrogen (N) use efficiency and reduce N-loss in rice paddy. Rhizosphere 30, 100875.

Kritee, K., Sigman, D.M., Granger, J., Ward, B.B., Jayakumar, A., Deutsch, C., 2012. Reduced isotope fractionation by denitrification under conditions relevant to the ocean. Geochim. Cosmochim. Acta 92, 243–259.

Li, X.M., Zhou, S.G., Li, F.B., Wu, C.Y., Zhuang, L., Xu, W., Liu, L., 2009. Fe(III) oxide reduction and carbon tetrachloride dechlorination by a newly isolated *Klebsiella pneumoniae* strain L17. J. Appl. Microbiol. 106, 130–139.

Liu, F., Rotaru, A.-E., Shrestha, P.M., Malvankar, N.S., Nevin, K.P., Lovley, D.R., 2012. Promoting direct interspecies electron transfer with activated carbon. Energy Environ. Sci. 5, 8982–8989.

Liu, T., Luo, X., Wu, Y., Reinfelder, J.R., Yuan, X., Li, X., Chen, D., Li, F., 2020. Extracellular electron shuttling mediated by soluble c-type cytochromes produced by *Shewanella oneidensis* MR-1. Environ. Sci. Technol. 54, 10577–10587.

Margalef-Marti, R., Bourbonnais, A., Knöller, K., Mayer, B., Altabet, M., Sebilo, M., 2026. Using N and O isotope fractionation for evaluating denitrification in aquatic systems. Trac. Trends Anal. Chem. 194, 118527.

Mariotti, A., Germon, J., Hubert, P., Kaiser, P., Letolle, R., Tardieux, A., Tardieux, P., 1981. Experimental determination of nitrogen kinetic isotope fractionation: some principles; illustration for the denitrification and nitrification processes. Plant and Soil 62, 413–430.

Martin, T.S., Casciotti, K.L., 2016. Nitrogen and oxygen isotopic fractionation during microbial nitrite reduction. Limnol. Oceanogr. 61, 1134–1143.

Pan, D., Chen, P., Yang, G., Niu, R., Bai, Y., Cheng, K., Huang, G., Liu, T., Li, X., Li, F., 2023. Fe(II) oxidation shaped functional genes and bacteria involved in denitrification and dissimilatory nitrate reduction to ammonium from different paddy soils. Environ. Sci. Technol. 57, 21156–21167 .

Pandey, C.B., Kumar, U., Kaviraj, M., Minick, K.J., Mishra, A.K., Singh, J.S., 2020. DNRA: a short-circuit in biological N-cycling to conserve nitrogen in terrestrial ecosystems. Sci. Total Environ. 738, 139710.

Saghaï, A., Hallin, S., 2024. Diversity and ecology of *NrfA*-dependent ammonifying microorganisms. Trends Microbiol. 32, 602–613.

Sigman, D.M., Casciotti, K.L., Andreani, M., Barford, C., Galanter, M., Böhlke, J., 2001. A bacterial method for the nitrogen isotopic analysis of nitrate in seawater and freshwater. Anal. Chem. 73, 4145–4153.

Simon, J., Gross, R., Einsle, O., Kroneck, P.M., Kröger, A., Klimmek, O., 2000. A NapC/NirT-type cytochrome c (NrfH) is the mediator between the quinone pool and the cytochrome *c* nitrite reductase of *Wolinella succinogenes*. Mol. Microbiol. 35, 686–696.

Stolz, J.F., Basu, P., 2002. Evolution of nitrate reductase: molecular and structural variations on a common function. Chem. Int. Chem. Biol. 3, 198–206.

Tischer, J., Zopfi, J., Frey, C., Venetz, J., Giglio, E., Burgdorfer, L., Rehmann, O., Wankel, S.D., Lehmann, M.F., 2026. Nitrogen and oxygen isotope effects during enzymatic nitrate reduction in vitro and by natural lake water consortia. Geochim. Cosmochim. Acta 423, 88–103.

Treibergs, L.A., Granger, J., 2017. Enzyme level N and O isotope effects of assimilatory and dissimilatory nitrate reduction. Limnol. Oceanogr. 62, 272–288.

Visser, A., Wankel, S., Frey, C., Kappler, A., Lehmann, M., 2022. Unchanged nitrate and nitrite isotope fractionation during heterotrophic and Fe(II)-mixotrophic denitrification suggest a non-enzymatic link between denitrification and Fe(II) oxidation. Front, Microbiol, p. 13.

Wang, S., Lyu, T., Li, S., Jiang, Z., Dang, Z., Zhu, X., Hu, W., Yue, F.-J., Ji, G., 2024. Unignorable enzyme-specific isotope fractionation for nitrate source identification in aquatic ecosystem. Chemosphere 348, 140771.

Wei, Z., Jin, K., Li, C., Wu, M., Shan, J., Yan, X., 2022. Environmental factors controlling dissimilatory nitrate reduction to ammonium in paddy soil. J. Soil Sci. Plant Nutr. 22, 4241–4248.